

# The empirical laws of galaxy dynamics: from gas kinematics to weak lensing

Federico Lelli<sup>1</sup>, Tobias Mistele<sup>2</sup>, Stacy S. McGaugh<sup>2</sup>, James M. Schombert<sup>3</sup>, and Pengfei Li<sup>4</sup>

<sup>1</sup>Arcetri Astrophysical Observatory, INAF, Largo Enrico Fermi 5, 50125, Florence, Italy

<sup>2</sup>Case Western Reserve University, 10900 Euclid Avenue, Cleveland, Ohio 44106, USA

<sup>3</sup>Department of Physics, University of Oregon, 1371 E 13th Ave, Eugene, Oregon 97403, USA

<sup>4</sup>School of Astronomy and Space Science, Nanjing University, Nanjing, Jiangsu 210023, China

**Abstract.** Galaxies obey a set of strict dynamical laws, which imply a close coupling between the visible matter (stars and gas) and the observed dynamics (set by dark matter in the standard cosmological context). Here we review recent results from weak gravitational lensing, which allow studying the empirical laws of galaxy dynamics out to exceedingly large radii in both late-type galaxies (LTGs) and early-type galaxies (ETGs). We focus on three laws: (1) the circular velocity curves of both LTGs and ETGs remain indefinitely flat out to several hundreds of kpc; (2) the same baryonic Tully-Fisher relation is followed by LTGs and ETGs; (3) the same radial acceleration relation (RAR) is followed by LTGs and ETGs. Combining galaxy data with Solar System data, the RAR covers about 16 orders of magnitude in the Newtonian baryonic acceleration. Remarkably, these empirical facts were predicted a priori by MOND.

## 1. Introduction

Galaxies display remarkable regularities in their dynamical properties, which can be summarized by a basic set of empirical laws:

1. **Flat Rotation Curves.** The circular velocity of a galaxy reaches an approximately constant value that persists indefinitely at large radii (Rubin et al. 1978; Bosma 1978).

2. **Renzo’s Rule.** For any feature in the circular-velocity curve of a galaxy, there is a corresponding feature in the baryonic density profile, and vice versa (Sancisi 2004).

3. **Baryonic Tully-Fisher Relation (BTFR).** At large radii, the “flat” circular speed correlates with the total baryonic mass (McGaugh et al. 2000; Lelli et al. 2019).

4. **Central Density Relation (CDR).** At small radii, the central dynamical surface density correlates with the central baryonic surface density (Lelli et al. 2013, 2016).

5. **Radial Acceleration Relation (RAR).** At each radius, the observed acceleration correlates with the baryonic acceleration (McGaugh et al. 2016; Lelli et al. 2017).

The term “circular velocity” ( $V_c$ ) refers to the rotation speed of a test particle on a circular orbit under the gravitational potential ( $\Phi$ ), so that  $V_c^2 = -R \cdot \partial_R \Phi$  where  $R$  is a cylindrical radius. In McGaugh et al. (2020) and Lelli (2022), we reviewed these laws focusing on kinematic data. In this review, after recalling some basic facts, we focus on weak gravitational lensing data.

In the particle dark matter (DM) context, each one of the dynamical laws implies a different type of baryon-DM coupling and/or fine-tuning problem in galaxy formation:

1. The asymptotic flatness of rotation curves implies that the radially-declining baryonic contribution ( $V_{\text{bar}}$ ) and the radially-rising DM contribution ( $V_{\text{DM}}$ ) must be fine-tuned in order to have  $V_{\text{bar}}(R)^2 + V_{\text{DM}}(R)^2 = \text{const}$  at each  $R$ . This is historically referred to as “disk-halo conspiracy” (van Albada & Sancisi 1986) and remains a problem for  $\Lambda$ CDM models of galaxy formation (Desmond 2017; Desmond et al. 2019).

2. Renzo’s rule implies that local variations in the baryonic mass distribution correspond to local variations in the total gravitational potential, even when DM supposedly dominates, so that baryons and DM must be locally coupled (Sancisi 2004).

3. The BTFR implies that the *global* baryonic-to-DM mass ratio ( $f_{\text{bar}} = M_{\text{bar}}/M_{\text{DM}}$ ) must systematically vary across galaxies with virtually no intrinsic scatter at a given mass, despite the stochastic process of galaxy formation (e.g., Desmond 2017). In addition, the lack of residual correlations with mean baryonic surface density ( $\Sigma_{\text{bar}}$ ) requires that  $\Sigma_{\text{bar}} \cdot f_{\text{bar}} = \text{const}$  at fixed mass, which is another fine-tuning problem.

4. The CDR implies that the *central* baryonic-to-DM ratio in galaxies must systematically vary with  $\Sigma_{\text{b}}(0)$ , with a characteristic “break” below which DM starts to dominate. In addition, the lack of residual correlations with total mass is puzzling because Newton’s shell theorem does not hold for a disk, so the dynamical surface density at small radii should depend also on the mass distribution at large radii (Lelli et al. 2016).

5. The RAR implies that the *local* baryonic-to-DM ratio at each  $R$  systematically depends on the Newtonian baryonic acceleration ( $g_{\text{bar}}$ ), with a characteristic acceleration scale below which DM starts to dominate. In addition, the lack of residual correlations with other galaxy properties is puzzling because, in a galaxy disk,  $g_{\text{bar}}(R)$  is given by a complex integral of the baryonic surface density at every  $R$  (Casertano 1983).

The BTFR, CDR, and RAR imply the existence of three logically distinct acceleration scales, each one playing a different role in galaxy dynamics (Lelli 2022). These acceleration scales, however, display a consistent value of  $\sim 10^{-10} \text{ m s}^{-2}$ , suggesting a common origin.

In the context of Milgromian dynamics (MOND, Milgrom 1983a,b), the acceleration scales are identified with a new constant of Nature,  $a_0$ , which sets the transition from the high-acceleration Newtonian regime to the low-acceleration Milgromian regime. Then, the dynamical laws can be derived from the basic tenets of MOND (Milgrom 2014). Actually, most of them were predicted by MOND in advance of the observations (McGaugh 2020).

The empirical laws of galaxy dynamics have been mostly studied in late-type galaxies (LTGs; spirals and dwarf irregulars) because they usually possess a rotation-supported gas disk with negligible pressure support, so that the circular velocity is directly probed by the observed rotation speeds. Early-type galaxies (ETGs; elliptical and lenticulars) may occasionally host rotation-supported gas disks (den Heijer et al. 2015), but it is more common to measure their circular velocities by modeling the stellar kinematics (considering both rotation and pressure support, e.g., Cappellari 2016) or the hydrostatic equilibrium of the X-ray gas halos (e.g., Buote & Humphrey 2012). These different methods indicate that ETGs generally follow the same dynamical laws as LTGs (den Heijer et al. 2015; Lelli et al. 2017; Shelest & Lelli 2020).

In the following, we review recent results from galaxy-galaxy weak gravitational lensing, which allow us to study the dynamical laws (1), (3), and (5) in both LTGs and ETGs out to exceedingly large radii: several hundreds of kpc.

## 2. Galaxy dynamics from weak gravitational lensing

### 2.1. The method

Gravitational lensing is sensitive to the total gravitational field of massive objects, so it can be used to study galaxy dynamics (Brouwer et al. 2021). Weak gravitational lensing measures little distortions induced by a “lens” on many background “source” galaxies. In practice, one measures the ellipticities of the source galaxies and infer the tangential shear  $\gamma_{\text{t}}$  by azimuthal averaging within a given projected radii  $R_{\text{p}}$  from the lens galaxy. The lensing signal induced by an individual galaxy, however, is weak, so one must stack

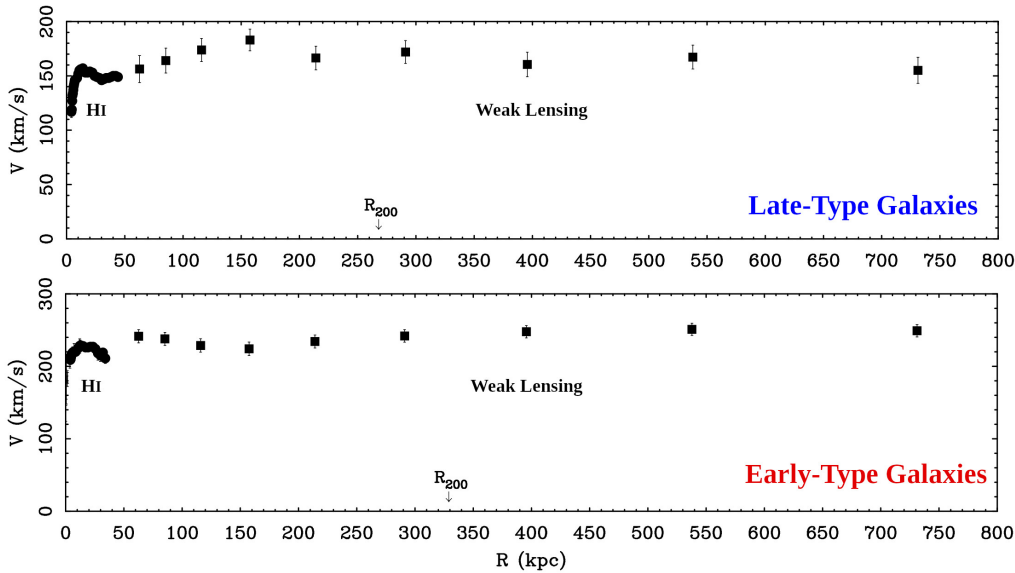


**Figure 1.** The circular velocities from weak lensing data (squares with errorbars) remain constant out to hundreds of kpc, well beyond the virial radius ( $R_{200}$ ) of their expected DM halos (Mistele et al. 2024a). The same phenomenology is seen in both LTGs (top) and ETGs (bottom). For reference, the circles at  $R < 50$  kpc show the HI rotation curves of two individual galaxies with similar masses as the lensing ensemble: the Sc NGC 3198 (top, from Begeman 1989) and the S0 UGC 6786 (bottom, from Noordermeer et al. 2007).

over tens of thousands of lenses. During the stacking, the intrinsic ellipticities of the source galaxies are averaged out, so that one probes only the actual lensing distortions. Commonly,  $\gamma_t$  is used to calculate the so-called excess mass surface density ( $\Delta\Sigma$ ).

Assuming spherical symmetry, Mistele et al. (2024b) derived a new formula to convert  $\Delta\Sigma$  into the observed acceleration ( $g_{\text{obs}}$ ) produced by the total mass distribution:

$$g_{\text{obs}}(r) = \frac{V_c^2(r)}{r} = 4G_N \int_0^{\pi/2} \Delta\Sigma \left( \frac{r}{\sin(\theta)} \right) d\theta, \quad (2.1)$$

where  $G_N$  is Newton's constant and  $r$  is the spherical radius. The average  $g_{\text{obs}}(r)$  can then be inferred by staking in bins of galaxy type, mass, or both (Mistele et al. 2024a,b).

Eq. 2.1 is expected to be valid in any metric theory where the matter fields (such as baryons and photons) are minimally coupled to the metric, so that in the quasi-static weak-field limit the metric has the same form as in General Relativity, just with a different gravitational potential than Newton's. A technical complication of Eq. 2.1 is that the integral requires measurements for  $R_p \rightarrow \infty$ , so we need to extrapolate the data beyond the last available measurement of  $\Delta\Sigma$ . This extrapolation sets the radial range of applicability of the method. Using KiDS data (Brouwer et al. 2021), Mistele et al. (2024a,b) found that the extrapolation becomes significant beyond  $\sim 1$  Mpc, so measurements of  $g_{\text{obs}}$  at  $r > 1$  Mpc are not considered. Another technical issue is that we aim to measure the average  $g_{\text{obs}}(r)$  of individual galaxies, so we need to select only isolated lenses before stacking their signals. To this aim, Mistele et al. (2024a,b) considered only lenses that have no other galaxy with more than 10% of their stellar mass within 4 Mpc.

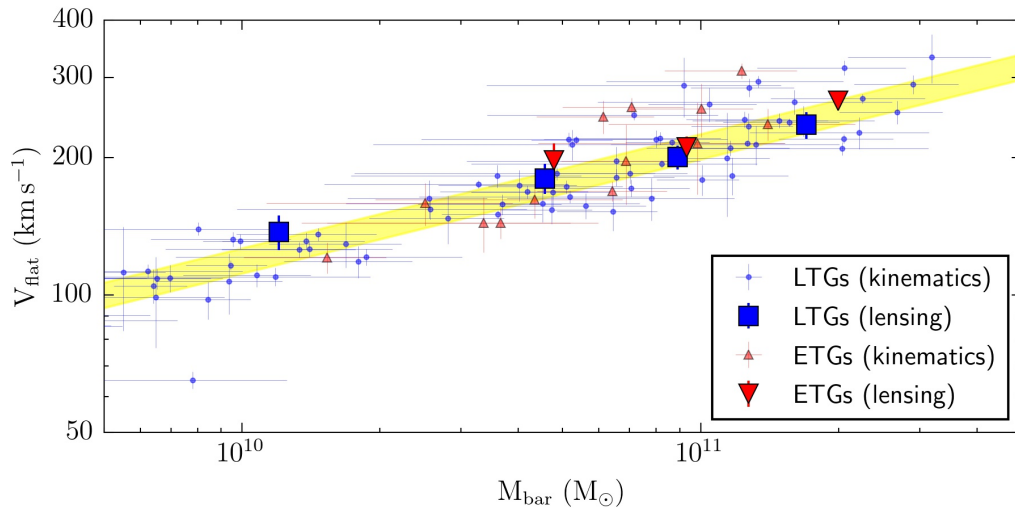


**Figure 2.** The BTFR focusing on the mass range  $M_{\text{bar}} = 5 \times 10^9 - 5 \times 10^{11} M_{\odot}$ . Large symbols show statistical weak lensing measurements for LTGs (blue squares) and ETGs (red down-triangles) from Mistele et al. (2024a). Small symbols show individual galaxies with kinematic data; LTGs (blue circles) from Lelli et al. (2019) and ETGs (red up-triangles) from den Heijer et al. (2015). The yellow band shows the MOND prediction considering a 25% error on  $a_0$ .

### 2.2. Indefinitely flat rotation curves

Figure 1 shows the circular velocities from KiDS DR4 weak-lensing data (Mistele et al. 2024a), measured for LTGs and ETGs separately. For both galaxy types, the circular velocities remain approximately flat for several hundreds of kpc. This enormously extends the classic result from HI rotation curves (Bosma 1978; van Albada & Sancisi 1986).

In the  $\Lambda$ CDM context, the flat part of the circular velocity curves extends well beyond the expected virial radius of the DM halos, where we would expect to see a Keplerian decline (see also Fig. 2 in Mistele et al. 2024a). In principle, a way to obtain such flat rotation curves in  $\Lambda$ CDM is to assume that the lenses are not sufficiently isolated (despite the strict isolation criterion) and that the contributions due to neighboring DM halos (the so-called “two-halo term”) have the right shape and amplitude to produce a constant  $V_c(r)$ . This approach raises a new “two-halo conspiracy” analogous to the classic “disk-halo conspiracy” at small radii (van Albada & Sancisi 1986): the declining contribution of the one-halo term ( $V_{\text{DM},1}$ ) needs to conspire with the rising contribution of the two-halo term ( $V_{\text{DM},2}$ ) such that  $V_{\text{DM},1}^2(R) + V_{\text{DM},2}^2(R) = \text{const}$  at large radii. In other words, the neighboring DM halos should arrange themselves around the primary halo in a fine-tuned way to make the circular velocity flat. This scenario appears quite contrived.

In the MOND context, the circular velocities of isolated systems are predicted to remain constant at large radii because the equations of motion become scale-invariant at low accelerations (Milgrom 2009). For non-isolated systems, instead, MOND predicts a mild decline due to the external field effect (Chae et al. 2020, 2021). The isolation criterion adopted by Mistele et al. (2024b,a) seems strict enough to avoid a significant external field effect from both nearby neighbors and the large-scale structure of the Universe.

### 2.3. Baryonic Tully-Fisher relation

Figure 2 shows the BTFR considering individual galaxies with kinematic data (den Heijer et al. 2015; Lelli et al. 2017, 2019) together with the statistical weak lensing measurements (Mistele et al. 2024a). The two different datasets are fully consistent with each other.

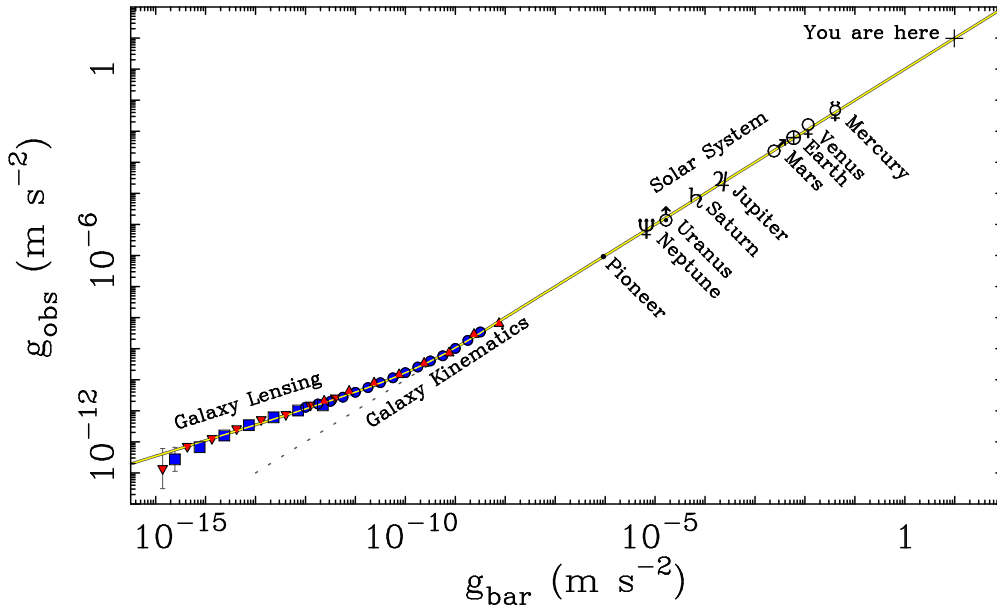


**Figure 3.** The RAR over the widest possible dynamic range:  $\sim 16$  orders of magnitude in  $g_{\text{bar}}$ . Symbols at high accelerations (where  $g_{\text{bar}} = g_{\text{obs}}$ ) show Earth’s surface gravity, the mean orbital acceleration of planets in the Solar System, and the farthest measured acceleration of the Pioneer spacecraft. Symbols at low accelerations show kinematic data for LTGs (blue circles) and ETGs (red up-triangles), and lensing data for LTGs (blue squares) and ETGs (red down-triangles). At accelerations below  $\sim 10^{-10} \text{ m s}^{-2}$ , the data display the DM effect ( $g_{\text{bar}} \neq g_{\text{obs}}$ ) and follow the relation  $g_{\text{obs}} = \sqrt{a_0 g_{\text{bar}}}$  (yellow line) predicted a-priori by MOND for isolated systems.

In the  $\Lambda$ CDM context, the BTFR must be the end result of the haphazard process of galaxy evolution. Thus, it is far from trivial to have LTGs and ETGs on the same relation because the two galaxy populations surely had different evolutionary histories (different merging histories, gas accretion histories, star-formation histories, and so on).

In the MOND context, the BTFR is a “Natural Law” with a fixed slope of 4. The yellow band in Fig. 2 shows the MOND prediction considering current uncertainties in the value of  $a_0$  (Lelli 2022). The data are clearly consistent with the MOND prediction.

#### 2.4. Radial Acceleration Relation

Figure 3 shows the RAR over the widest possible range, from the Earth’s surface gravity to the outermost parts of galaxies. The kinematic data of galaxies probe the range  $10^{-8} - 10^{-12} \text{ m s}^{-2}$  in  $g_{\text{bar}}$ , while weak lensing data the range  $10^{-12} - 10^{-15} \text{ m s}^{-2}$ . Empirically, the DM effect ( $g_{\text{obs}} > g_{\text{bar}}$ ) kicks in at  $\sim 10^{-10} \text{ m s}^{-2}$ . This value is 4 orders of magnitude smaller than the lowest acceleration where Newtonian dynamics has been directly tested in non-relativistic systems, corresponding to the outermost parts of the Solar System.

The RAR has two acceleration scales: one setting the transition  $g_{\text{obs}} > g_{\text{bar}}$  and one setting the overall normalization. Remarkably, the two acceleration scales coincide within the errors, so we have been referring to them as  $g_{\dagger}$  (see Sect. 3.2 in Lelli et al. 2017). The bottom portion of the RAR implies  $g_{\text{obs}} = \sqrt{g_{\dagger} g_{\text{bar}}}$ , which is mathematically equivalent to a BTFR with slope of 4 and no radial dependencies (see Sect. 7.1 in Lelli et al. 2017).

In the  $\Lambda$ CDM context, the physics that may set these acceleration scales is unclear; a possibility is to assume that the star-formation efficiency of galaxies is related to the gravitational potential (Grudić et al. 2020). Importantly, the weak lensing data at  $g_{\text{bar}} \lesssim$

$10^{-12} - 10^{-13} \text{ m s}^{-2}$  reach beyond the virial radius of the DM halo (Fig. 1), so one expects that the data should bend below the relation  $g_{\text{obs}} = \sqrt{g_{\dagger} g_{\text{bar}}}$  and follow the Newtonian prediction rescaled by the galaxy baryon fraction,  $g_{\text{obs}} = f_{\text{bar}} g_{\text{bar}}$ . This basic expectation has been confirmed by  $\Lambda$ CDM simulations (Mercado et al. 2024) but is not seen in the lensing data, which instead follows precisely the extrapolation of the kinematic data.

In a MOND context,  $g_{\dagger}$  is identified with  $a_0$ , which was historically determined using other methods (Milgrom 1983a,b). MOND predicts that the data should follow the relation  $g_{\text{obs}} = \sqrt{a_0 g_{\text{bar}}}$  down to low accelerations (as observed), as long as galaxies are sufficiently isolated for the external field effect to be negligible (Chae et al. 2020, 2021).

### 3. Conclusions

Weak gravitational lensing data allows extending the empirical laws of galaxy dynamics out to very large radii and low accelerations. These empirical laws are difficult to understand in the  $\Lambda$ CDM context. Remarkably, they were predicted a-priori by MOND.

### References

- Begeman, K. G. 1989, *A&A*, 223, 47  
 Bosma, A. 1978, PhD thesis, University of Groningen  
 Brouwer, M. M., Oman, K. A., Valentijn, E. A., et al. 2021, *A&A*, 650, A113  
 Buote, D. A. & Humphrey, P. J. 2012, in *Astrophysics and Space Science Library*, Vol. 378, 235  
 Cappellari, M. 2016, *ARA&A*, 54, 597  
 Casertano, S. 1983, *MNRAS*, 203, 735  
 Chae, K.-H., Desmond, H., Lelli, F., McGaugh, S. S., & Schombert, J. M. 2021, *ApJ*, 921, 104  
 Chae, K.-H., Lelli, F., Desmond, H., et al. 2020, *ApJ*, 904, 51  
 den Heijer, M., Oosterloo, T. A., Serra, P., et al. 2015, *A&A*, 581, A98  
 Desmond, H. 2017, *MNRAS*, 472, L35  
 Desmond, H., Katz, H., Lelli, F., & McGaugh, S. 2019, *MNRAS*, 484, 239  
 Grudić, M. Y., Boylan-Kolchin, M., Faucher-Giguère, C.-A., & Hopkins, P. F. 2020, *MNRAS*, 496, L127  
 Lelli, F. 2022, *Nature Astronomy*, 6, 35  
 Lelli, F., Fraternali, F., & Verheijen, M. 2013, *MNRAS*, 433, L30  
 Lelli, F., McGaugh, S. S., Schombert, J. M., Desmond, H., & Katz, H. 2019, *MNRAS*, 484, 3267  
 Lelli, F., McGaugh, S. S., Schombert, J. M., & Pawlowski, M. S. 2016, *ApJ*, 827, L19  
 Lelli, F., McGaugh, S. S., Schombert, J. M., & Pawlowski, M. S. 2017, *ApJ*, 836, 152  
 McGaugh, S. 2020, *Galaxies*, 8, 35  
 McGaugh, S., Lelli, F., Li, P., & Schombert, J. 2020, in *IAU Symposium*, Vol. 353, *Galactic Dynamics in the Era of Large Surveys*, ed. M. Valluri & J. A. Sellwood, 144–151  
 McGaugh, S. S., Lelli, F., & Schombert, J. M. 2016, *PRL*, 117, 201101  
 McGaugh, S. S., Schombert, J. M., Bothun, G. D., & de Blok, W. J. G. 2000, *ApJ*, 533, L99  
 Mercado, F. J., Bullock, J. S., Moreno, J., et al. 2024, *MNRAS*, 530, 1349  
 Milgrom, M. 1983a, *ApJ*, 270, 371  
 Milgrom, M. 1983b, *ApJ*, 270, 365  
 Milgrom, M. 2009, *ApJ*, 698, 1630  
 Milgrom, M. 2014, *MNRAS*, 437, 2531  
 Mistele, T., McGaugh, S., Lelli, F., Schombert, J., & Li, P. 2024a, *ApJL*, 969, L3  
 Mistele, T., McGaugh, S., Lelli, F., Schombert, J., & Li, P. 2024b, *JCAP*, 2024, 020  
 Noordermeer, E., van der Hulst, J. M., Sancisi, R., et al. 2007, *MNRAS*, 376, 1513  
 Rubin, V. C., Thonnard, N., & Ford, Jr., W. K. 1978, *ApJ*, 225, L107  
 Sancisi, R. 2004, in *IAU Symposia*, Vol. 220, *Dark Matter in Galaxies*, 233  
 Shelest, A. & Lelli, F. 2020, *A&A*, 641, A31  
 van Albada, T. S. & Sancisi, R. 1986, *Royal Soc. of London Phil. Transac. Series A*, 320, 447